RSC Advances

ROYAL SOCIETY OF CHEMISTRY

PAPER

View Article Online
View Journal | View Issue

Cite this: *RSC Adv.*, 2016, **6**, 77440

Published on 11 August 2016. Downloaded by FAC DE QUIMICA on 15/06/2017 21:00:24.

Combined study of the effect of deposition temperature and post-deposition annealing on the photoluminescence of silicon quantum dots embedded in chlorinated silicon nitride thin films†

M. A. Serrano-Núñez,[a] A. Rodríguez-Gómez,*[b] L. Escobar-Alarcón[c] and J. C. Alonso-Huitrón[a]

Chlorinated-silicon nitride (SiN_x:Cl) thin films with embedded silicon quantum dots (Si-QDs) were grown by remote plasma enhanced chemical vapor deposition using SiH_2Cl_2, H_2, NH_3 and Ar at different deposition temperatures (DT) in the range of 50 to 350 °C and using steps of 50 °C. After that, each sample was subjected to annealing treatments at temperatures (AT) of 400, 700 and 1000 °C. The evolution of the optical properties, composition and structure as a function of DT and AT were investigated by Null Ellipsometry, photoluminescence (PL) measurements, UV-Vis spectroscopy, X-ray Photoelectron Spectroscopy (XPS), Fourier Transform Infrared Spectroscopy (FTIR), scanning electron microscopy with energy-dispersive X-ray spectroscopy (SEM) with (EDS) and High Resolution Transmission Electron Microscopy (HRTEM). A red-shift in the PL peak and an increment in the PL integrated intensity of the films was found on increasing DT from 150 to 350 °C; such changes can be explained by modifications of the matrix chemical composition and by the quantum confinement effect due to an increase in the size and density of Si-QDs respectively. A chemical analysis revealed that films deposited below 150 °C suffer a post-deposition oxidation process leading to the formation of silicon oxide; this process is accelerated by the temperature of the annealing treatment. Meanwhile films deposited between 150 and 350 °C are mainly composed of silicon nitride that diminishes the mentioned oxidation due to the thermal treatments and promotes the splitting of Si-QDs into two populations with different average diameter. The annealed films deposited below 150 °C show a clearly decrement in the PL intensity, meanwhile the maximum emission PL peak from annealed films grown from 150 to 350 °C shifts to high emission energies. This post thermal annealing blue-shift can be mainly related to the nucleation of new small Si-QDs. We concluded that temperature is one of the most important mainstays to achieve good luminescence from Si-QDs.

Received 17th June 2016
Accepted 11th August 2016

DOI: 10.1039/c6ra15723h

www.rsc.org/advances

1. Introduction

Silicon (in crystalline or amorphous form) is the most important semiconductor in the microelectronics and photovoltaic industries.[1,2] Unfortunately, its poor radiative efficiency due to an indirect band gap limits its use in photonic applications.[3] Nonetheless, silicon is capable of emitting light in the visible range when it is in the form of nanostructures such as silicon quantum dots embedded in a silicon-based dielectric matrix.[4–12] Numerous research groups are working on developing EL structures based on Si-QDs for miscellaneous applications,[1,13–17] and it is expected that such structures would be used in artificial-light silicon devices, optical communications, and lasers, which could revolutionize the actual photoelectronic technology.[1,2,18–20]

Nowadays the growth of Si-QDs at low temperatures is a challenge, but the benefits of achieving this goal are multiples, for example, the possible application in very large scale integration (VLSI) devices. In VLSI devices the low temperatures are useful to avoid unwanted diffusion at the interfaces of multilayered structures.[21] Additionally, low-temperature fabrication processes could lead to the fabrication of innovative electronic devices deposited over transparent soft substrates with low melting points, such as those used for flexible solar cells and full-color flat panel displays.[22]

In order to find different ways to approach the temperature challenge, some research groups have started to prepare semiconductor quantum dots by chemical wet technologies due to

[a]*Instituto de Investigaciones en Materiales, Universidad Nacional Autónoma de México, Ciudad Universitaria, AP 70-360, Coyoacán 04510, México DF, Mexico*

[b]*Instituto de Física, Universidad Nacional Autónoma de México, A.P. 20-364, Coyoacán 01000, México DF, Mexico. E-mail: arodriguez@fisica.unam.mx*

[c]*Departamento de Física, Instituto Nacional de Investigaciones Nucleares, Apdo. Postal 18-1027, México DF 11801, Mexico*

† Electronic supplementary information (ESI) available. See DOI: 10.1039/c6ra15723h

This journal is © The Royal Society of Chemistry 2016

Published on 11 August 2016. Downloaded by FAC DE QUIMICA on 15/06/2017 21:00:24.

their low cost and compatibility with flexible plastic substrates.[23,24] Nevertheless, wet techniques are not fully compatible with the silicon microelectronic industry, thence it is necessary to continue exploring the possibility of preparing silicon quantum dots, silicon nanocrystals and silicon nanoclusters, at lower temperatures using industrially-compatible techniques such as plasma enhanced chemical vapor deposition (PECVD). Furthermore, it is worth to mention that dry techniques allow the growth of silicon nitride thin films with better optical and structural quality than chemical techniques.[25,26] In this sense, it is important to recall that when is used in electroluminescent (EL) structures, silicon nitride (SiN_x) is one of the best silicon dielectric matrix due to its medium to high carrier mobility and low-energy barrier height, which could allow the fabrication of devices at lower turn-on voltage than other silicon insulators.[2,11,12]

There are few studies about the influence of deposition temperature (DT) on Si-QDs embedded in a silicon based insulator matrix prepared by PECVD. One of them reports the study of the deposition of amorphous silicon carbide (SiC) films at DT in the range of 80 to 575 °C, the authors shows that the formation of SiC nanocrystals starts at 300 °C.[27] Other recent study reports tunable visible PL from Si-QD as a function of DT.[28] On the other hand, in regard to the effect of temperature on Si-QDs after deposition, several groups have reported significant post annealing changes on the photoluminescence from Si-QDs embedded in a silicon nitride matrix deposited between 200 and 300 °C.[12,29–31]

Temperature is a parameter of great importance in the conformation of SiQDs, for that reason there is a good amount of studies related to substrate temperature, and other similar amount related to annealing temperatures, all of them looking for the successful formation of silicon nanoparticles and the control of their photoluminescence. However, to our best knowledge there is none work that studies the two parameters at the same time.

In this paper, we have carried out an innovative combined study of the effects the annealing temperature (AT) has on Si-QDs embedded in a chlorinated silicon nitride matrix (SiN_x:Cl) deposited by remote PECVD at different substrate temperatures (DT). We made a comprehensive analysis of the structural, chemical and optical properties of the samples at different DT and AT. These results throw light on the behavior of the growth of Si-QDs in a chlorinated silicon nitride matrix as a function of DT, and the evolution of the matrix composition and its luminescence as a function of AT. We observed that temperature during the growing or after the deposition is one of the most important mainstays to achieve good luminescence (integrated intensity and tunable maximum peaks) from Si-QDs.

2. Experimental details

The films of Si-QDs embedded in chlorinated-silicon nitride were prepared in a RPECVD system whose characteristics are described elsewhere.[32] The films were grown on p-type (100) low resistivity (5–10 Ω cm) silicon substrates and quartz substrates. Prior to deposition, silicon substrates were dipped in "p-etch solution" (300 : 15 : 10 parts of $H_2O : HNO_3 : HF$) for 2 min to remove native oxide, and rinsed with deionized water. The quartz substrates were solvent cleaned with trichloroethylene, methanol and acetone. The deposition parameters were: a chamber pressure of 300 mTorr, a radio frequency power (13.56 MHz) of 150 watts, and a gas mixture of SiH_2Cl_2, H_2, NH_3 and Ar with flow rates of 5, 20, 200 and 75 sccm, respectively. The DT was varied from 50 to 350 °C in steps of 50 °C. After deposition, the films were cut into small pieces and annealed at AT of 400, 700 and 1000 °C for 30 minutes.

The thickness and refractive index of the films were measured by null ellipsometry using a manual Gaertner L117 ellipsometer equipped with a He–Ne laser (λ = 632.8 nm) at an incidence angle of 70°. PL spectra of the films were recorded with a Fluoromax-Spex spectrofluorometer in a dark room at room temperature by exciting with a Kimmon He–Cd laser beam with λ = 325 nm (3.81 eV) and a power of 25 mW. Ultraviolet-visible (UV-vis) transmission measurements were carried out using a double-beam PerkinElmer Lambda 35 UV-vis spectrophotometer in the range of 190 to 1100 nm. Surface chemical analysis of the as grown films was carried out by X-ray photoelectron spectroscopy (XPS) using a K-Alpha Thermo Scientific spectrometer (Al-Kα X-ray of 1486.68 eV), employing a hemispherical analyzer. Chemical bond analysis was performed using a Fourier Transform Infrared Spectrophotometer (FTIR) Nicolet 210 operated in the range of 400–4000 cm^{-1} with a resolution of 2 cm^{-1}. The surface morphology of the as-grown samples was studied by atomic force microscopy (AFM) using a Jeol JSPM-4210 on tapping mode and a high resolution Mikromasch NSC15 silicon tip with radius of curvature <10 nm. Measurements of cluster diameter, height and number density were made using the WinSPM, DPS Version 2.00. Scanning Electron Microscopy was carried out using a Schottky field emission ultra-high resolution Scanning Electron Microscope JEOL-JSM-7800F equipped with Oxford Instruments EDS detector and AZtec 2.1 software. The existence of Si-QDs in a few samples was confirmed by High-Resolution Transmission Electron Microscopy (HRTEM) using a JEOL JEM-2010F FasTEM microscope which operates at 200 kV near the Scherrer focus, with a theoretical point to point resolution of 0.19 nm. The HRTEM images in planar view were recorded with a CCD camera and processed with a GATAN digital micrograph system Version 3.7.0. The samples were thinned for electron transparency by mechanic grinding using a tripod polisher (South Bay Technology model 590 TEM), and by ion milling (ion polishing system GATAN model 691).

3. Results and discussion

3.1 Chemical and morphological analysis

The Fig. 1 shows that spectra of films deposited below 200 °C exhibit the presence of $Si–NH_2$ bonds related to absorption bands located around 2150, 3040, 2820 and 1415 cm^{-1}.[33,34] On the other hand, the spectra of films deposited at DT in the range of 200 to 350 °C exhibit a main absorption band located around 865 cm^{-1} corresponding to stretching vibrations of Si–N bonds,

Published on 11 August 2016. Downloaded by FAC DE QUIMICA on 15/06/2017 21:00:24.

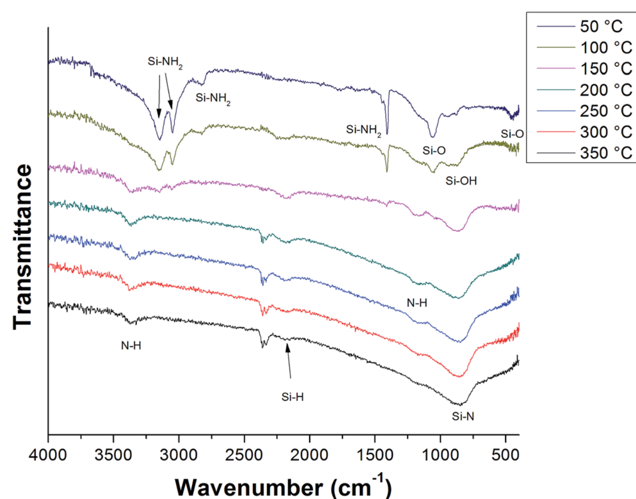

Fig. 1 FTIR transmission spectra of as-grown films deposited at DT in the range of 50 to 350 °C. It is identified that aminosilanes disappear in all those films grown with temperatures above the 150 °C.

which is a first indication that these films are mainly composed by silicon nitride.[33–35] The above can be explained as follows: during the gas-phase process of a deposition using SiH_2Cl_2 and NH_3 as precursor gases, the dominant chemical reactions are:[36]

$$SiH_2Cl_2 + NH_3 \xrightarrow{\text{plasma}} SiH_2(NH_2)Cl + HCl\uparrow \quad (1)$$

$$SiH_2Cl_2 + NH_3 \xrightarrow{\text{plasma}} SiH(NH_2)Cl_2 + H_2\uparrow \quad (2)$$

The H_2 and HCl are eliminated by the insertion of amino groups as can be seen from eqn (1) and (2). This could lead to the formation of a plasma with high content of aminosilanes ($Si(NH_2)_x$) until it reaches $Si(NH_2)_4$. Subsequently, during the surface reaction process a chemical condensation of the adsorbed radicals can occur, forming silicon nitride when increasing DT by means of mechanisms as the one described as follows by Smith *et al.*:[37]

$$3Si(NH_2)_4 \xrightarrow{\text{heat}} Si_3N_4 + 8NH_3\uparrow \quad (3)$$

For a better understanding of the growth process we performed an XPS analysis of the films with different DT. Table 1 shows that N/Si ratio of the as-grown films increases when DT also increases. This observed increment in the N/Si ratio and the reduction of Si–NH_2 bonds when increasing DT is in accordance with the proposed mechanism in eqn (3). It is possible to note that N/Si ratio is lower than the characteristic value of 1.33 for stoichiometric silicon nitride (Si_3N_4), which means that our as-deposited films are silicon-rich. In the same way, the value of refractive index of as-grown films showed in the Fig. S1† increases with a raise in DT and tends to 2, which is the characteristic value of Si_3N_4.

Table 1 N/Si ratio and Cl at% of as-grown films deposited in the range from 50 to 350 °C

DT (°C)	N/Si ratio	Cl at%
50	0.04	0.7
100	0.06	0.8
150	0.09	1.0
200	0.21	1.3
250	0.79	4.3
300	0.94	4.4
350	0.91	3.5

Additionally, it is possible to identify from Fig. 1 that films deposited at DT of 50 to 150 °C show absorption bands located around 1060 and 450 cm^{-1} corresponding to stretching and rocking vibrations of Si–O bonds respectively[34,38] and the absorption band located at 940 cm is related to Si–OH bonds.[34,35] Since these films were deposited in a well-isolated vacuum system using precursor gases different than oxygen or its compounds, the clear presence of oxygen in our thin films is due to post-deposition transformations.[34] These transformations could be attributed to a great incorporation of chlorine in the as-deposited films which means a considerable amount of Si–Cl terminal bonds that causes open film networks with a high porosity as can be noted by SEM image shown in Fig. 2, then when these permeable films are exposed to ambient, it could produce the diffusion of moisture into the films causing its hydrolization by means of chemical reactions between unstable Si–Cl bonds and water molecules as:[38]

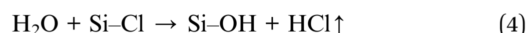

$$H_2O + Si\text{–}Cl \rightarrow Si\text{–}OH + HCl\uparrow \quad (4)$$

The volatile HCl produced by this process can easily escape to the ambient, which can explain the low Cl content of the as-deposited films. The presence of Cl in small quantities was observed by XPS analysis as shown in Table 1. Evidence of

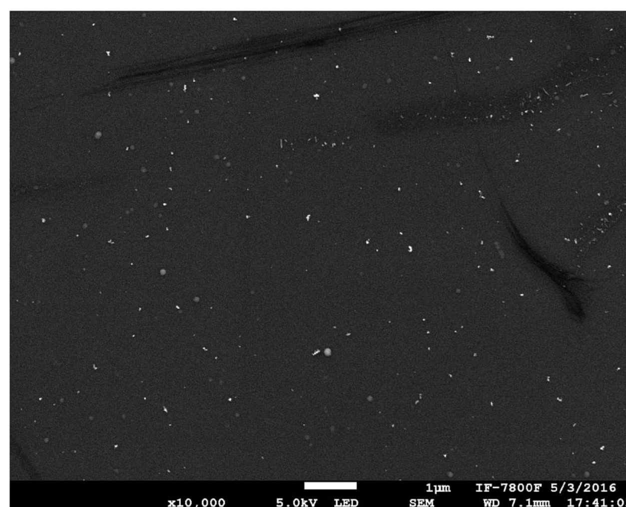

Fig. 2 SEM image of a film deposited at DT of 50 °C – AT: N/A. This film exhibit a low surface quality in terms of roughness and apparent porosity; it is possible to distinguish small scratches on the surface due to handling. These damages are also observable on the surfaces of samples DT: 100 °C – AT: 700 °C and DT: 100 °C – AT: 1000 °C.

This journal is © The Royal Society of Chemistry 2016

Published on 11 August 2016. Downloaded by FAC DE QUIMICA on 15/06/2017 21:00:24.

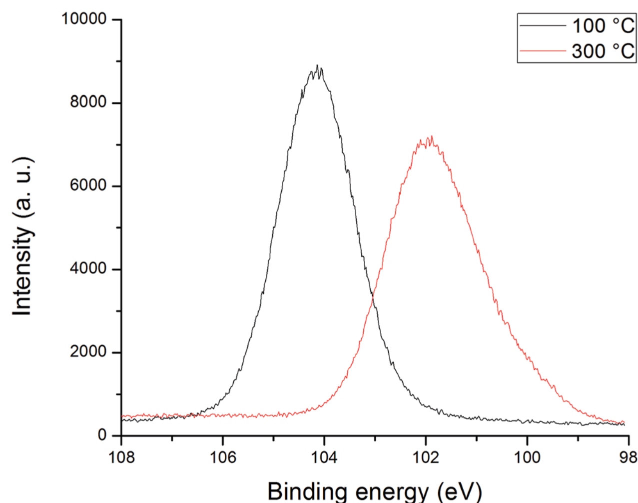

Fig. 3 Si 2p core-level spectra for as-deposited films grown at DT of 100 and 300 °C. After de analysis of the observed binding energies, it is possible to infer that films deposited under 200 °C are composed by oxy-nitrides while above 200 °C are composed by SiN_x.

hydrolysis has been found at the surface of films deposited at low DT after ambient exposure for a few minutes where an off-white thin layer appears instantly, which causes unexpected thicker films as shown in Fig. S2.†

The Si 2p core-level spectra for the as-grown films deposited at DT of 100 and 300 °C can be observed in Fig. 3. The binding energy of 104 eV corresponds to the sample DT: 100 °C – AT: 0 °C (and is the same for all depositions made with DT below 200 °C). Meanwhile, the sample DT: 300 °C – AT: 0 °C exhibit a peak around 102 eV (same for all films with DT in the 200–350 °C range). For SiN_x, a previous study showed that the Si 2p core-level spectra shifted from a binding energy of 99.6 eV at $x = 0$ (pure silicon) to 102.8 eV at $x = 1.5$.[39] In the case of SiO_x, other study revealed a shift from 99.6 eV for $x = 0$ to 104 eV at $x = 2$ (SiO_2).[40] Hence, it is possible for us to state that our films deposited at DT below 150 °C are mainly composed by oxy-nitrides, on the other hand, the films prepared in the range from 200 to 350 °C have a SiN_x composition with oscillating x values.

FTIR spectra of films deposited at DT of 100 and 300 °C are shown in Fig. 4(a) and (b) respectively, before and after thermal annealing at AT of 400, 700 and 1000 °C. Fig. 4(a) clearly shows a phase transition from a complex mixture of aminosilanes and oxygen-related compounds to SiO_x for the film grown at 100 °C after thermal annealing. Moreover, the value of refractive index after annealing tends to 1.47, which corresponds to a characteristic value of SiO_2. The described transition could be due to the diffusion of surface oxygen into the film and this evolution in the matrix was also observed for the film deposited with DT below 200 °C. Fig. 4(b) evidently shows that films deposited at DT of 300 °C are principally composed of SiN_x even after thermal annealing of 400, 700 and 1000 °C. In addition, this figure shows the post annealing attenuation of absorption bands located at 2200 cm^{-1} related to stretching vibrations of Si–H bonds,[34,35] and 3360 and 1160 cm^{-1} related to stretching and bending N–H bonds respectively.[33–35] The evident attenuation of these absorption bands could be due to the effusion of hydrogen from the film until hydrogen cannot be appreciated after thermal annealing of 1000 °C. This behavior occurs for films prepared with DT from 200 to 350 °C.

The matrix in which the Si-QDs are embedded is of fundamental importance since their quality significantly influence the absorption-emission characteristics of the system. In order to study the morphological properties and chemical composition of all our samples we have carried out a comprehensive analysis by scanning electron microscopy (SEM) and energy dispersive X-ray spectroscopy (EDS).

The first step for element quantification by EDS was an unrestricted elemental analysis, *i.e.* quantification of all characteristic X-rays from any element present in the sample or even X-rays originated by pollutant elements coming from the process of sample preparation for electron microscope observation. In the unrestricted elemental analysis of all our samples we found three elements of greater presence: Si, N and O. The

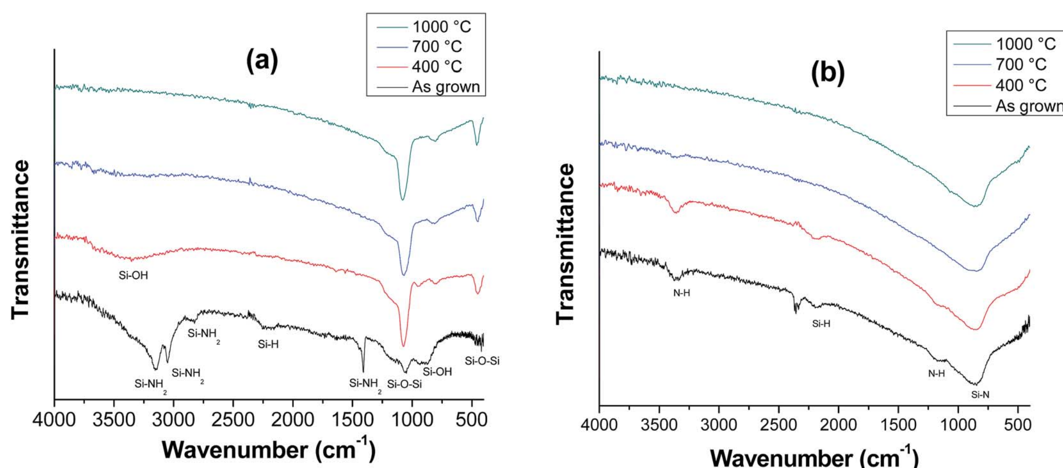

Fig. 4 FTIR transmission spectra of a film deposited at (a) 100 °C, and (b) 300 °C, before and after of thermal annealing at 400, 700 and 1000 °C. The absorption band located around 3600 to 3300 cm^{-1} in spectrum of Fig. 2(a) annealed at 400 °C corresponds to Si–OH bonds.[38]

Published on 11 August 2016. Downloaded by FAC DE QUIMICA on 15/06/2017 21:00:24.

sum of the mass percent composition (wt%) of Si, N and O ranged from 94% for sample DT: 250 °C – AT: 400 °C up to 97% for sample DT: 150 °C – AT: 700 °C. It is important to state that the sum of the wt% does not represent the way in which the constituent elements (Si, N and O) are distributed, but it can be understood as a reliability factor of the compositional measurement. For example, the sample DT: 50 °C – AT: 1000 °C had the following values obtained from an unrestricted elemental analysis: Si = 49.05%, O = 47.61%, C = 2.18%, other elements = 1.16%. In this case nitrogen is not present but the sum Si + N + O is 96.6% and remains up than 94%.

After the elemental analysis without restriction, we performed an EDS analysis with restriction, *i.e.* we only quantified Si, N and O to obtain 100% in the elemental analysis. Regarding reliability due to equipment sensitivity, we report for each compositional analysis the value of the standard deviation (σ wt%). When the value of wt% is greater than 3σ wt% then the level of confidence in the measurement is of 99.7%.

The Fig. 5(a) shows the cross-sectional micrograph of the sample DT: 50 °C – AT: 1000 °C and (b) the cross-sectional micrograph of sample DT: 50 °C – AT: N/A. By using backscattered electron detector one can clearly identify the presence and uniformity of the film for the sample DT: 50 °C – AT: 1000 °C which has thicknesses ranging from 76 and 82.5 nm. Film uniformity is an indicator that oxidation process due to the annealing treatment is not forming interfaces, but rather the oxygen diffuses into the film uniformly. Interestingly, the fluctuation in film thickness ($\approx$6.5 nm) is the biggest observed for all our samples, the latter makes us to deduct that the oxidation process consumes small portions of the film.

All the cross sectional composition analyses exhibited small variations of the constituent elements mass fractions (Si, N and O). To clearly indicate the above is enough to say that in 21 out of 28 analyzes, the silicon mass fraction fluctuated between 70% and 71%, with slight variations of O and N in the remaining 29–30%. Therefore, we decided to implement an analysis method that allows us to observe compositional trends more easily. This analysis method compares the composition of the film against stoichiometric silicon dioxide (SiO_2 → Si = 46.74%, O = 53.26%) and silicon nitride (Si_3N_4 → Si = 60.06%, N = 39.94%).

To explain the operation of our analysis let's take the sample DT: 200 °C – AT: 700 °C from Table 2. Within the box one can read: dioxide-like: 9.6%, nitride-like: 55.2%; however, compositional analysis for this sample was: Si = 72.85%, N = 22.04%, O = 5.11%. For calculating the similarities with silicon dioxide or silicon nitride we used a rule of three that compares the oxygen and nitride content against stoichiometric SiO_2 and Si_3N_4. Hence, if an oxygen mass fraction of 60.06% has 100% of similitude with SiO_2, then an oxygen mass fraction of 5.11% has a similitude with SiO_2 of 9.6%. The same applies for the nitrogen, a mass fraction of 39.94% has 100% of similitude with Si_3N_4, and therefore 22.04% of nitrogen is similar to stoichiometric silicon nitride by an amount of 55.2%.

We want to warn the reader that these similarities must not be taken in a verbatim way. The carried out analysis is just a tool that allows us to discharge in Table 2 all compositional analyzes in a simple and compact way. Additionally, it is possible to clearly identify the oxygen incorporation habit on our films depending on deposition temperature and annealing temperature. In this regard, we can observe that annealing treatments allow oxygen incorporation on the film regardless its deposition temperature; as bigger the AT the bigger the oxygen incorporation at any DT. Nevertheless, one can observe even a bigger oxygen incorporation due to annealing treatments in those films with DT of 50 °C, 100 °C *y* 150 °C.

We can conjecture that deposition temperature allows an adequate film conformation – consolidation due to the mobility of the precursor species reacting over the substrate. This

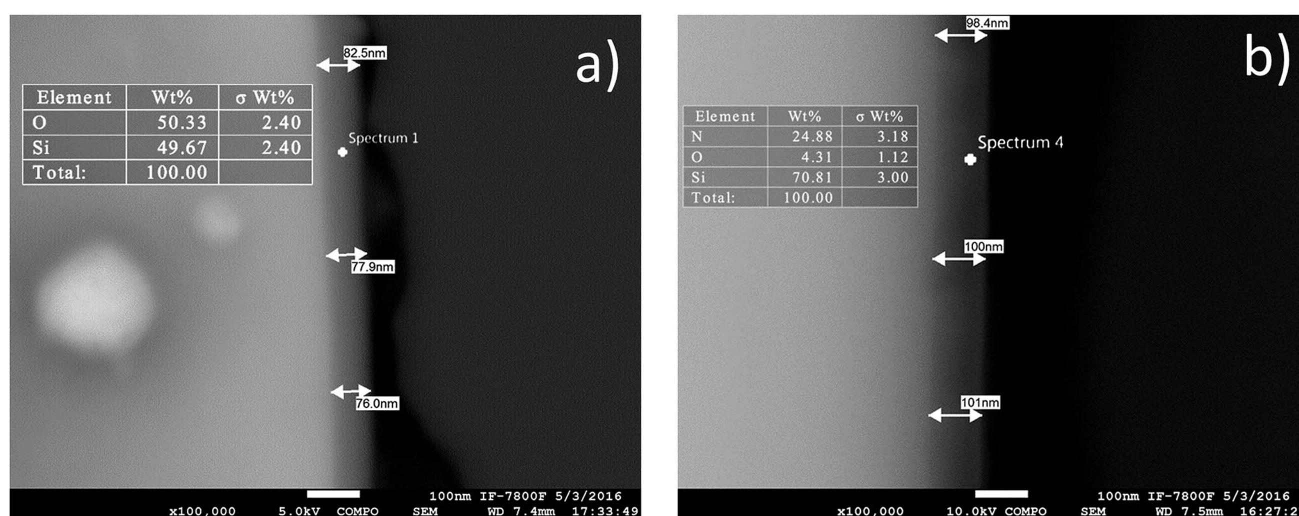

Fig. 5 (a) Cross sectional SEM images of sample DT: 50 °C – AT: 1000 °C at 100 000×. A point over the film indicates the location where EDS was performed, the elemental composition table is included. It is possible to observe the uniformity of the film that ranges from 76 to 82 nm thick. This image illustrates the followed methodology to perform the elemental analysis on the film edge for the 28 samples under study. (b) Cross sectional SEM micrograph of sample DT: 300 °C – AT: N/A. Location of the EDS analysis and elemental composition table are included. Thin film is very homogenous, it has thicknesses between 98 and 101 nm.

 This journal is © The Royal Society of Chemistry 2016

Published on 11 August 2016. Downloaded by FAC DE QUIMICA on 15/06/2017 21:00:24.

Table 2 Cross sectional compositional analyses of all samples under study. Analyses are expressed using the comparison method between sample composition and stoichiometric silicon dioxide and silicon nitride. It is possible to observe the oxygen incorporation trend with annealing temperature

DT (°C)/AT (°C)	N/A	400	700	1000
50	Dioxide-like: 57.4% Nitride-like: 12.4%	Dioxide-like: 69.1% Nitride-like: 9.0%	Dioxide-like: 86.4% Nitride-like: 9.8%	Dioxide-like: 94.4% Nitride: nondescript
100	Dioxide-like: 42.4% Nitride-like: 15.8%	Dioxide-like: 70.8% Nitride-like: 12.1%	Dioxide-like: 92.6% Nitride-like: nondescript	Dioxide-like: 94.2% Nitride-like: nondescript
150	Dioxide-like: 18.6% Nitride-like: 41.8%	Dioxide-like: 21.6% Nitride-like: 40.2%	Dioxide-like: 21.8% Nitride-like: 41.1%	Dioxide-like: 24.3% Nitride-like: 39.4%
200	Dioxide-like: 9.8% Nitride-like: 58.4%	Dioxide-like: 7.6% Nitride-like: 57.1%	Dioxide-like: 9.6% Nitride-like: 55.2%	Dioxide-like: 12.1% Nitride-like: 53.4%
250	Dioxide-like: 8.3% Nitride-like: 60.2%	Dioxide-like: 9.3% Nitride-like: 59.2%	Dioxide-like: 9.9% Nitride-like: 57.0%	Dioxide-like: 13.7% Nitride-like: 55.6%
300	Dioxide-like: 8.1% Nitride-like: 62.3%	Dioxide-like: 9.2% Nitride-like: 62.0%	Dioxide-like: 9.6% Nitride-like: 62.1%	Dioxide-like: 10.4% Nitride-like: 60.8%
350	Dioxide-like: 8.3% Nitride-like: 61.8%	Dioxide-like: 9.8% Nitride-like: 60.9%	Dioxide-like: 10.5% Nitride-like: 60.5%	Dioxide-like: 11.0% Nitride-like: 59.7%

consolidation could be interpreted as a better quality silicon nitride film that prevents the formation of oxy-nitrides that are more easily formed in the films with deposition temperatures between 50 and 150 °C. However, the formation of oxy-nitrides cannot be totally avoided since the oxygen incorporation is inherent of silicon-based compounds that are exposed to the environment (including monocrystalline silicon wafers). In a summarized manner, we can conclude that the deposition temperature is related to the quality of silicon nitride to be formed, the annealing temperature is related to the incorporation of oxygen after nitride formation, and there is going to be greater oxygen incorporation in low quality silicon nitrides.

3.2 Absorption analysis

The optical transmission spectra of samples deposited on fused silica substrates were measured by UV-Vis spectroscopy in order to study the optical band gap (E_g). It is well known that for this purpose, the Tauc model is widely used to estimate E_g of amorphous materials such as SiN_x or SiO_x. Considering the approximation of indirect transitions, Tauc model is given by:[41,42]

$$(\alpha h\nu)^{\frac{1}{2}} = A\left(h\nu - E_g\right) \quad (5)$$

where $h\nu$ is the photon energy, A is the Tauc constant, and α is the absorption of the films. Fig. 6 shows the Tauc plots, $(\alpha h\nu)^{1/2}$ *vs.* $h\nu$, of the as-grown films deposited from 50 to 350 °C. In a previous work the presence of maximums and minimums in the Tauc plots (multiple peaks) have been discussed and attributed to constructive and destructive interference due to the thickness of these films.[32] We can estimate E_g by extrapolating to zero ordinate a straight line fitted to the main slope observed in Tauc plots. The obtained values of E_g for as-deposited films prepared using temperatures from 200 to 350 °C are shown in the inset table of Fig. 6. It is important to observe that those E_g values are lower than the silicon nitride band gap ($E_g = 5.3$ eV), which means that they can be associated to a great number of Si–Si bonds replacing Si–N bonds in a silicon-rich silicon nitride matrix of the films.[25] Since some authors state that Tauc plots can present uncertainty in the determination of E_g due to an energy-dependent slope,[43] we have also obtained E_g for as-grown films using Cody plots as can be seen in Fig. S3,†[44] the values of E_g estimated by Tauc plots (around 4.2 eV) are higher than those estimated by Cody plots (around 3.9 eV). The determination of E_g is empirical by either Cody or Tauc methods, therefore is certain extent devious to opt for one another, however we believe that the widespread of Tauc model makes it more valuable for comparison purposes. It is worth to note that E_g of films deposited with DT below 200 °C cannot be obtained by either Tauc or Cody plots because they do not show any region for a linear fit.

The E_g of as-grown films deposited from 50 to 150 °C cannot be obtained due to their low optical transmission as can be seen in UV-Vis transmission spectra shown in Fig. S4.† In consideration of the high porosity of these samples as mentioned before, it could be possible that the network of our films are filled of defects as dangling bonds which could lead to a high absorption in the UV-Vis range. Additionally to this, and in order to explore the possibility of low transmission due to scattering

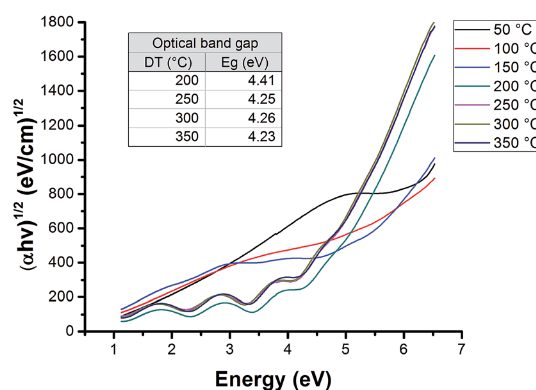

Fig. 6 Tauc plots of as-grown films prepared at DT from 50 to 350 °C. Inset table presents the optical band gap of films grown in the 200–350 °C range.

Published on 11 August 2016. Downloaded by FAC DE QUIMICA on 15/06/2017 21:00:24.

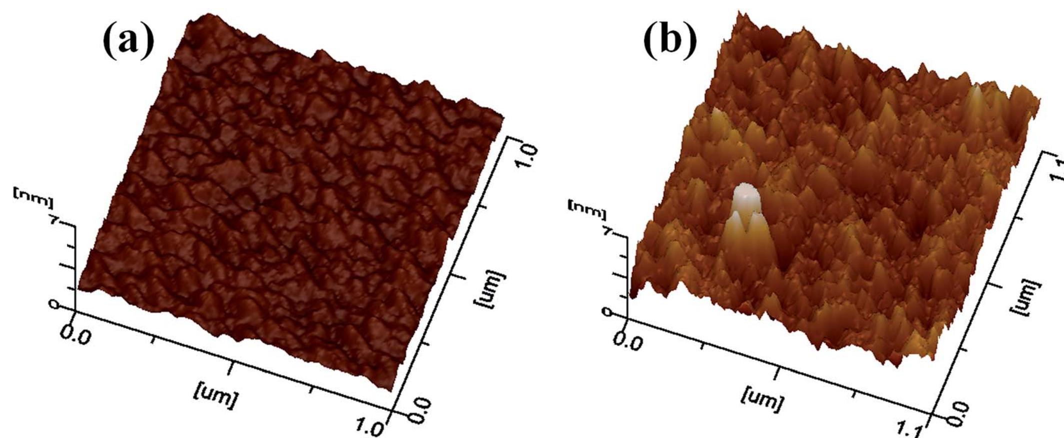

Fig. 7 AFM micrographs of as-grown films deposited at DT of (a) 300 °C, and (b) 100 °C. The top of the height (z) scale was set at 7 nm.

losses generated by rough surfaces we carried out a surface morphological study by AFM of sample DT: 100 °C – AT: N/A and DT: 300 °C – AT: N/A. Fig. 7 shows a smooth surface for the film deposited at DT of 300 °C, while the film deposited at 100 °C exhibit the formation of a great number of small pillars. The surface roughness depth of film deposited at 100 °C (around 6.6 nm) is higher compared with the roughness of the film prepared at 300 °C (around 1.6 nm). However, it is clear that such a big variation of the absorption properties cannot be attributed to scattering from 6.6 nm rough surface.

3.3 Emission analysis

In the last decades the luminescence of new silicon-based materials has been exhaustively studied. In order to explain this phenomenon researchers have developed emission models such as quantum confinement effect (QCM),[7–10,45] or radiative defect-related states at the silicon-based matrix and the Si-QD interface.[31,46–49] Although both models can successfully explain the luminescence from silicon systems we cannot forget the entanglement between quantum confinement, quantum dot passivation and matrix chemical composition. In this study, the chemical composition of the matrix is changing as a function of DT and AT. This compositional change is also promoting a change in the passivation of Si-QDs population. It is evident that these variations generate deep changes in the emission characteristics of the sample, possibly these variations are responsible for the biggest changes in the emission characteristics of our samples. However, quantify these two parameters is beyond our reach due the uncertainties in the compositional analysis of the matrices and the impossibility to verify the manner in which the Si-QDs were passivated. We have therefore decided to analyze more deeply the influence that the quantum dot size and density have on the luminescence characteristics, while being aware that luminescence changes are not only due to these two characteristics.

The room temperature PL spectra in the visible range of our as-deposited films are displayed in Fig. 8, the PL clearly shows an increase in the intensity as DT increases. The PL spectra of films deposited at 50 and 100 °C have de same E_{PL} and full width at medium half (FWHM) but different intensity. Since these films are mainly composed of oxy-nitrides we can attribute their PL to Si=O double bonds at the Si-QD interface or SiO_x matrix instead of QCM.[46,48,49] The normalized PL spectra of our as-deposited films are shown in Fig. 9. It can be observed that films prepared from 150 to 350 °C are tunable (in a very short range) as we increase DT, so the PL of these films can be related to radiative recombination of electron–hole pairs in Si-QDs, and according to QCM the E_{PL} is being tuned mainly by a variation in the confinement d.

The quantum confinement effect model (QCM) relates the peak at maximum PL intensity (E_{PL}) with the band gap of the Si-QDs.[7–10,25,38–40,45] When silicon is confined, the band gap becomes quasi-direct and increases as the Si-QDs size decreases below the Bohr radius of excitons (~5.3 nm).[50] The QCM considers a particle with an effective mass m^* confined in a cubic rigid box with side of length d and assumes infinite potential barriers, so the band gap energy for three dimensionally confined Si-QDs can be expressed as follows:

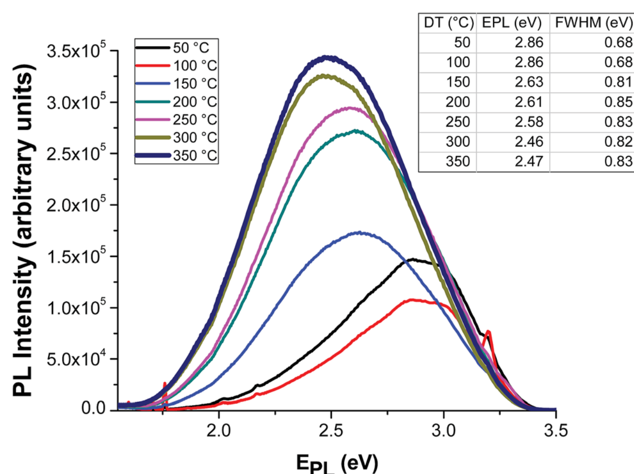

DT (°C)	EPL (eV)	FWHM (eV)
50	2.86	0.68
100	2.86	0.68
150	2.63	0.81
200	2.61	0.85
250	2.58	0.83
300	2.46	0.82
350	2.47	0.83

Fig. 8 Room temperature PL spectra of as-grown films deposited at DT of 50 to 350 °C. Inset table shows the energy (E_{PL}) of the peaks and the full width at medium half (FWHM) of all the as-grown samples.

 This journal is © The Royal Society of Chemistry 2016

Published on 11 August 2016. Downloaded by FAC DE QUIMICA on 15/06/2017 21:00:24.

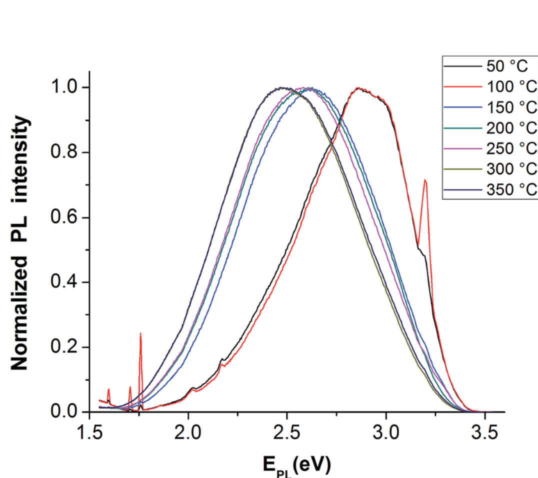

Fig. 9 Normalized PL spectra of as-grown films deposited at DT of 50 to 350 °C.

$$E_{PL}\ (\text{eV}) = E_{Si} + \frac{C}{d^2} \tag{6}$$

where $E_{Si} = 1.6$ eV is the band gap energy of bulk Si, C is the quantum confinement parameter (dependent of m^*), and d is the diameter of the Si-QDs in nanometers.

In previous studies, we reported the fabrication of Si-QDs (with tunable average size) by means of varying deposition parameters and using the same RPECVD equipment used in this work.[9,32,34,51–53] Therefore, we estimate the existence of embedded Si-QDs in all our as-grown films, nevertheless it is of fundamental importance to confirm this existence in at least one of our as-deposited films with the purpose of make some conjectures regarding the characteristics of the nanoclusters.

The Fig. 10 shows a HRTEM image obtained from the sample DT: 300 °C – AT: N/A, it is possible to observe the presence of Si-QDs. Nevertheless, it is not clear in our HRTEM analysis if the Si-QDs are crystalline or amorphous; in the one by one Si-QDs counting we could not identify many reticular patterns

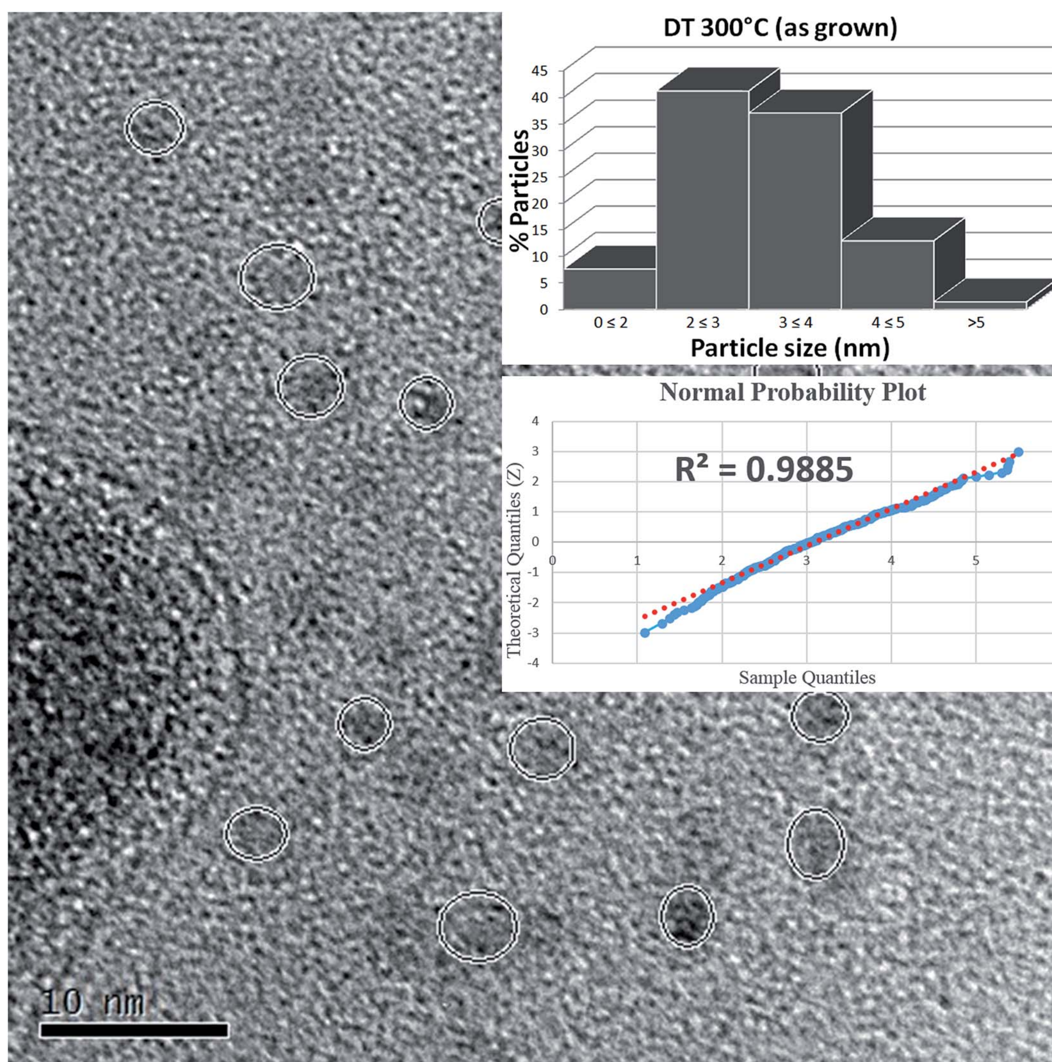

Fig. 10 HRTEM image of Si-QDs embedded in an as-deposited film prepared at 300 °C. The circles indicate some Si-QDs of different size embedded in the film. The insets of the image are part of the statistical analysis of the Si-QD population of this sample.

Published on 11 August 2016. Downloaded by FAC DE QUIMICA on 15/06/2017 21:00:24.

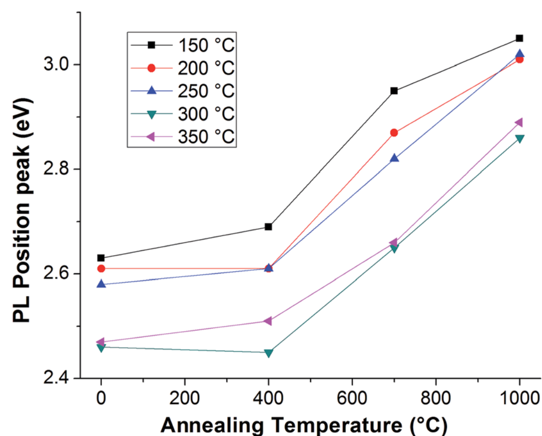

Fig. 11 PL position peaks of films deposited at DT in the range of 150 to 350 °C, before and after thermal annealing at AT of 400, 700 and 1000 °C. A blue-shift after thermal annealing of 700 and 1000 °C can be observed clearly in all the films.

indicating crystallinity. Additionally, a previous theoretical study conducted by Nishio *et al.* reveals that amorphous silicon quantum dots (a-Si-QD) have a better radiative recombination rate and use to be smaller than crystalline Si-QDs.[54] Therefore we believe our Si-QDs population is mostly conformed by amorphous particles. A statistical analysis was done in order to determine the Si-QDs population characteristics. From a population of 4350 particles we found the following values, mean diameter value (μ): 3.1 nm, standard deviation (σ): 0.81 nm, Mean Absolute Deviation (MAD): 0.65 nm and particle density (ρ) of 2.91 $\times$ 10^{11} particles per cm^2. The histogram for this sample is presented as an inset in the Fig. 10, and together with the normal probability plot (also displayed as an inset in Fig. 10) is possible to observe a normal distribution of the Si-QDs population.

If we assume that each deposited film at its respective DT has different μ and ρ, we can describe by using the QCM the relationship between the PL and the characteristics of Si-QDs population in each film as function of DT. The decrease in

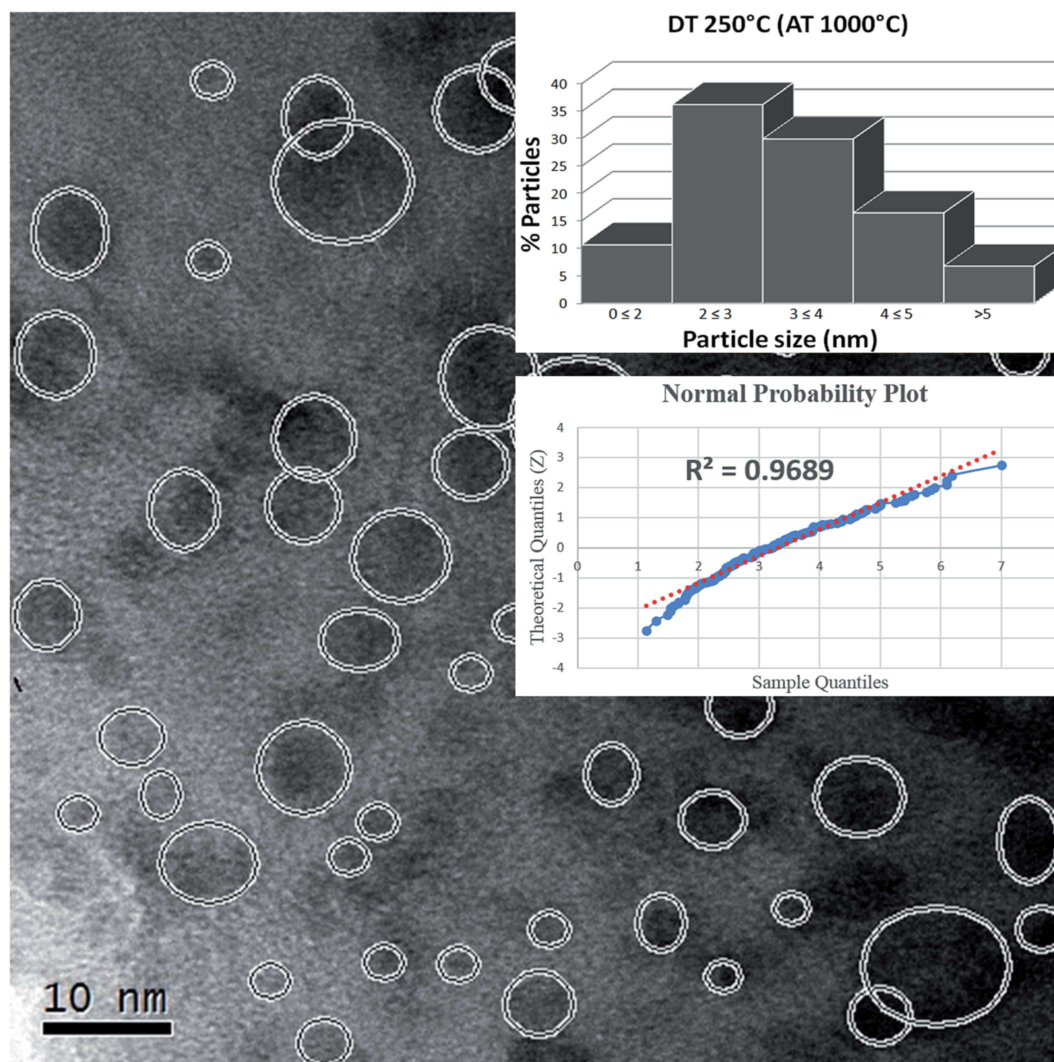

Fig. 12 HRTEM image of a film deposited at 250 °C and annealed at 1000 °C. The white circles indicate some Si-QDs of different size in the film. The inset image is a statistical analysis of the Si-QD size embedded in the film.

 This journal is © The Royal Society of Chemistry 2016

Published on 11 August 2016. Downloaded by FAC DE QUIMICA on 15/06/2017 21:00:24.

E_{PL} and the increase of PL integrated intensity as DT increases is due to an increment in μ and ρ. The FWHMs of the films deposited from 150 to 350 °C are around ~0.81–0.85 eV, which means that the size distribution of these films follows a normal distribution and is quite similar for all samples.

The evolution of the photoluminescence of the films as function of annealing temperature was studied for each as-grown film at its respective DT. The PL spectra of as-grown and annealed films at AT of 400, 700 and 1000 °C deposited at DT in the range of 50 to 350 °C are shown in Fig. S5–S11.† The films deposited at 50 and 100 °C evidently show a decrease in the PL intensity after thermal annealing, which as mentioned above cannot be related to radiative recombinations of electron–hole pairs in Si-QDs. In the case of samples deposited in the range from 150 to 350 °C, the PL shows an enhancement with a thermal annealing of 400 °C which could be due to an improvement of the structure by eliminating non-radiative defects, whereas the films annealed at 700 and 1000 °C show a shift to higher energies of E_{PL} as can be seen in Fig. 11. Based on QCM, this blue-shift should be related to a splitting into two Si-QDs populations: the formation of new small amorphous Si-QDs which emit photons of high energy,[7,12,23,30,31] and the broaden of the existing Si-QDs until sizes larger than the Bohr radius.

To throw light on the phenomenon of particle size variation we carried out a HRTEM analysis of the sample prepared at DT of 250 °C and annealed at 1000 °C. In Fig. 12 we can qualitatively observe large non-confined Si-QDs (responsible of the quenching of the PL integrated intensity), and new small confined Si-QDs which can be related to the blue-shift of the E_{PL}. The statistical parameters of this sample are: population 2070 particles, mean diameter value (μ): 3.3 nm, standard deviation (σ): 1.1 nm, Mean Absolute Deviation (MAD): 0.88 nm and particle density (ρ) of 1.30×10^{12} particles per cm^2. The normal probability plot included as an inset in Fig. 12 indicates a good approximation to the normal distribution, however it is possible to observe normality deviations in the extremes of the population, which is a good indicator of the splitting of Si-QDs population. From the histogram displayed as an inset of Fig. 12 can be observed the formation of new small particles, *i.e.* the percentage of particles between 1 and 2 nm have increased from ≈7% to almost 11%. Additionally, it is notable the increment of particles bigger that 5 nm from ≈1.3% to ≈7% and a higher σ that confirms the Si-QD's population is changing in the manner we discussed above.

Finally, the decrease in the PL intensity of the Si-QDs embedded in as-deposited films after thermal annealing at 700 and 1000 °C could be due to the rupture of Si–H and Si–Cl bonds, which leads to the formation of electronic non-radiative defects in the Si-QDs surface. Since amorphous Si-QDs have a high radiative recombination rate than crystalline Si-QDs,[39,50,54] the crystallization of these Si-QDs embedded in films annealed at 1000 °C can affect the PL by reducing its intensity.

4. Conclusions

We have studied in two ways the temperature effect on the luminescence of Si-QDs, first the influence of the substrate growing temperature (DT) and second the effect of post deposition annealing temperature (AT), the Fig. 13 summarizes the findings of our work.

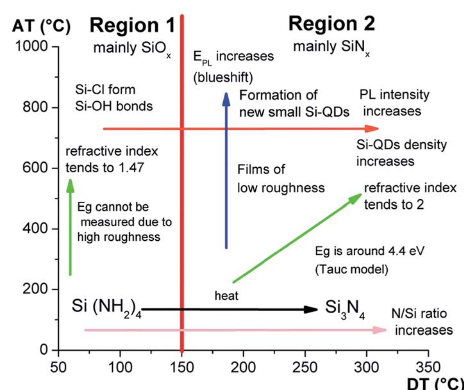

Fig. 13 The results from this paper are summarized in this AT-DT chart. Two regions are clearly defined by the DT 150 °C, in region 1 luminescence is poor and any annealing treatments worsens it. Meanwhile in region 2 luminescence is in concordance with the QCM and is changed by annealing treatments.

It is possible to identify the existence of two regions, in region 1 (50 °C to 150 °C) matrix is formed mostly by low quality silicon nitride (oxy-nitrides), in this region the AT annihilates the originally poor luminescence of the as-grown films. Meanwhile, region 2 (above 150 °C) shows an almost flawless matrix of silicon nitride, for this region the post deposition annealing improves the luminescence of the samples because the temperature creates new Si-QDs that make a blue-shift in the PL maximum intensity peak and generates an increasing in the PL integrated intensity. Additionally, we believe the matrix compositional changes are possible responsible of the biggest changes in the absorption-emission characteristics in our samples. We observed that low temperatures indeed allow the formation of some Si-QDs however, is the poor quality of the matrix the responsible of the low luminescence.

We can estimate that any PECVD system will have a threshold temperature in order to growth matrices that can promote the best luminescence from Si-QD. From our work it is also possible to conclude that manipulation of these nanostructures could be done in very simple systems by making a careful combination of parameters, which provides a wider perspective for the study and technologic transference of these nanostructures.

Acknowledgements

All authors would like to acknowledge the technical assistance from J. M. Garcia León, M. A. Canseco and Carlos Flores. Authors are also grateful to Dr Carlos Raul Magaña Zavala and Dr Samuel Tehuacanero Cuapa for their valuable assistance in operation and data interpretation of the JEOL-Schottky Field Emission Scanning Electron Microscope JSM-7800F. We also want to express our gratitude to Ing. María Cristina Zorrilla Cangas and M. en C. Manuel Aguilar Franco for technical

Published on 11 August 2016. Downloaded by FAC DE QUIMICA on 15/06/2017 21:00:24.

assistance in SEM-EDS analysis from Scanning Electron Microscope JEOL-5600LV, as well as the support received from L. D. Luis Novoa Sandoval for his assistance in the graphical organization of SEM images and Fís. Héctor de Jesús Cruz-Manjarrez Flores-Alonso for his advices regarding the vacuum systems used for this work. First author is grateful for the support received by the Mexican Council for Science and Technology (CONACyT-México) through the scholarship No. 295633. This work was partially supported by the project PAPIIT UNAM IG100614-2.

References

1 F. Priolo, T. Gregorkiewicz, M. Galli and T. F. Krauss, *Nat. Nanotechnol.*, 2014, **9**, 19–32.
2 J. C. Alonso, G. Santana, A. Benami and B. M. Monroy, *Encycl. Nanosci. Nanotechnol.*, 2011, 1–31.
3 L. Pavesi, *Mater. Today*, 2005, **8**, 18–25.
4 Z. T. Kang, B. Arnold, C. J. Summers and B. K. Wagner, *Nanotechnology*, 2006, **17**, 4477–4482.
5 B.-H. Lai, C.-H. Cheng, Y.-H. Pai and G.-R. Lin, *Opt. Express*, 2010, **18**, 4449.
6 G. Wen, X. Zeng, X. Wen and W. Liao, *J. Appl. Phys.*, 2014, **115**, 164303.
7 Y. Kurokawa, S. Tomita, S. Miyajima, A. Yamada and M. Konagai, *Jpn. J. Appl. Phys.*, 2007, **46**, L833–L835.
8 T.-W. Kim, C.-H. Cho, B.-H. Kim and S.-J. Park, *Appl. Phys. Lett.*, 2006, **88**, 123102.
9 A. Rodriguez, J. Arenas and J. C. Alonso, *J. Lumin.*, 2012, **132**, 2385–2389.
10 B. Sain and D. Das, *J. Lumin.*, 2015, **158**, 11–18.
11 M. Molinari, H. Rinnert and M. Vergnat, *J. Appl. Phys.*, 2007, **101**, 123532.
12 B. Sahu, F. Delachat, A. Slaoui, M. Carrada, G. Ferblantier and D. Muller, *Nanoscale Res. Lett.*, 2011, **6**, 178.
13 J. C. Alonso, F. A. Pulgarín, B. M. Monroy, A. Benami, M. Bizarro and A. Ortiz, *Thin Solid Films*, 2010, **518**, 3891–3893.
14 C.-H. Cheng, C.-L. Wu, C.-C. Chen, L.-H. Tsai, Y.-H. Lin and G.-R. Lin, *IEEE Photonics J.*, 2012, **4**, 1762–1775.
15 C.-H. Cheng, Y.-C. Lien, C.-L. Wu and G.-R. Lin, *Opt. Express*, 2013, **21**, 391.
16 H.-Y. Tai, Y.-H. Lin and G.-R. Lin, *IEEE Photonics J.*, 2013, **5**, 6600110.
17 Y. Xin, K. Nishio and K. Saitow, *Appl. Phys. Lett.*, 2015, **106**, 201102.
18 L. Canham, *Nature*, 2000, **408**, 411–412.
19 G. T. Reed, *Nature*, 2004, **427**, 595–596.
20 L. Pavesi, L. Dal Negro, C. Mazzoleni, G. Franzò and F. Priolo, *Nature*, 2000, **408**, 440–444.
21 K. Banerjee and S. Ikeda, in *Guide to State-of-the-Art Electron Devices*, John Wiley & Sons, Ltd, Chichester, UK, 2013, pp. 133–155.
22 X. Dai, Z. Zhang, Y. Jin, Y. Niu, H. Cao, X. Liang, L. Chen, J. Wang and X. Peng, *Nature*, 2014, **515**, 96–99.
23 Y. Shirasaki, G. J. Supran, M. G. Bawendi and V. Bulović, *Nat. Photonics*, 2012, **7**, 13–23.
24 M. K. Choi, J. Yang, K. Kang, D. C. Kim, C. Choi, C. Park, S. J. Kim, S. I. Chae, T.-H. Kim, J. H. Kim, T. Hyeon and D.-H. Kim, *Nat. Commun.*, 2015, **6**, 7149.
25 S.-L. Ku and C.-C. Lee, *Opt. Mater.*, 2010, **32**, 956–960.
26 B.-H. Liao and C.-N. Hsiao, *Appl. Opt.*, 2014, **53**, A377.
27 T. Rajagopalan, X. Wang, B. Lahlouh, C. Ramkumar, P. Dutta and S. Gangopadhyay, *J. Appl. Phys.*, 2003, **94**, 5252.
28 B. Sain and D. Das, *Phys. Chem. Chem. Phys.*, 2013, **15**, 3881.
29 W. Liao, X. Zeng, X. Wen, X. Chen and W. Wang, *Vacuum*, 2015, **121**, 147–151.
30 X. Zeng, W. Liao, G. Wen, X. Wen and W. Zheng, *J. Appl. Phys.*, 2014, **115**, 154314.
31 L. Jiang, X. Zeng and X. Zhang, *J. Non-Cryst. Solids*, 2011, **357**, 2187–2191.
32 A. Rodriguez-Goómez, A. Garciía-Valenzuela, E. Haro-Poniatowski and J. C. Alonso-Huitroón, *J. Appl. Phys.*, 2013, **113**, 233102.
33 G. Santana, J. Fandiño, A. Ortiz and J. C. Alonso, *J. Non-Cryst. Solids*, 2005, **351**, 922–928.
34 A. López-Suárez, J. Fandiño, B. M. Monroy, G. Santana and J. C. Alonso, *Phys. E*, 2008, **40**, 3141–3146.
35 G. Santana, B. M. Monroy, A. Ortiz, L. Huerta, J. C. Alonso, J. Fandiño, J. Aguilar-Hernaández, E. Hoyos, F. Cruz-Gandarilla and G. Contreras-Puentes, *Appl. Phys. Lett.*, 2006, **88**, 041916.
36 A. Bagatur'yants, K. Novoselov, A. Safonov, L. Savchenko, J. Cole and A. Korkin, *Mater. Sci. Semicond. Process.*, 2000, **3**, 23–29.
37 D. L. Smith, *J. Electrochem. Soc.*, 1990, **137**, 614.
38 V. P. J. C. Alonso, R. Vazquez and A. Ortiz, *J. Vac. Sci. Technol., A*, 1998, **16**, 3211.
39 R. Kärcher, L. Ley and R. L. Johnson, *Phys. Rev. B: Condens. Matter Mater. Phys.*, 1984, **30**, 1896–1910.
40 F. G. Bell and L. Ley, *Phys. Rev. B: Condens. Matter Mater. Phys.*, 1988, **37**, 8383–8393.
41 J. Tauc, *Amorphous and Liquid Semiconductors*, Plenum Press, New York, 1974.
42 S. Mirabella, R. Agosta, G. Franzó, I. Crupi, M. Miritello, R. Lo Savio, *et al.*, *J. Appl. Phys.*, 2009, **106**, DOI: 10.1063/1.3259430.
43 P. Liu, P. Longo, A. Zaslavsky and D. Pacifici, *J. Appl. Phys.*, 2016, **119**, 014304.
44 G. D. Cody, B. G. Brooks and B. Abeles, *Sol. Energy Mater.*, 1982, **8**, 231–240.
45 G. Franzò, M. Miritello, S. Boninelli, R. Lo Savio, M. G. Grimaldi, F. Priolo, F. Iacona, G. Nicotra, C. Spinella, S. Coffa, G. Franzò, M. Miritello, S. Boninelli, R. Lo Savio, M. G. Grimaldi and F. Priolo, *J. Appl. Phys.*, 2014, **094306**, 0–5.
46 C. Summonte, M. Allegrezza, M. Bellettato, F. Liscio, M. Canino, A. Desalvo, J. López-vidrier, S. Hernández, L. López-conesa, S. Estradé, F. Peiró and B. Garrido, *Sol. Energy Mater. Sol. Cells*, 2014, **128**, 138–149.
47 C. M. Mo, L. Zhang, C. Xie and T. Wang, *J. Appl. Phys.*, 1993, **73**, 5185–5188, DOI: 10.1063/1.353796.
48 Z. X. Cao, R. Song, L. B. Ma, Y. Du, A. L. Ji and Y. Q. Wang, *Nanotechnology*, 2006, **17**, 2073–2077.

 This journal is © The Royal Society of Chemistry 2016

49 A. Puzder, A. Williamson, J. Grossman and G. Galli, *Phys. Rev. Lett.*, 2002, **88**, 2–5.
50 P. Trwoga, A. Kenyon and C. Pitt, *J. Appl. Phys.*, 1998, **83**, 3789–3794.
51 A. Rodríguez, J. Arenas, A. L. Pérez-Martínez and J. C. Alonso, *Mater. Lett.*, 2014, **125**, 44–47.
52 A. López-Suárez, C. Torres-Torres, R. Rangel-Rojo, J. A. Reyes-Esqueda, G. Santana, J. C. Alonso, A. Ortiz and A. Oliver, *Opt. Express*, 2009, **17**, 10056–10068.
53 A. L. Muñoz-Rosas, A. Rodríguez-Gómez, J. A. Arenas-Alatorre and J. C. Alonso-Huitrón, *RSC Adv.*, 2015, **5**, 92923–92931.
54 K. Nishio, J. Kōga, T. Yamaguchi and F. Yonezawa, *Phys. Rev. B: Condens. Matter Mater. Phys.*, 2003, **67**, 1–5.

Published on 11 August 2016. Downloaded by FAC DE QUIMICA on 15/06/2017 21:00:24.